ANALYSIS OF INDUCTION-TYPE COILGUN PERFORMANCE BASED ON CYLINDRICAL CURRENT SHEET MODEL

J. L. He, E. Levi, Z. Zabar, L. Birenbaum and Y. Naot

Polytechnic University
333 Jay Street, Brooklyn, NY 11201

ABSTRACT

This paper presents a method based on a cylindrical current sheet model for the analysis and design of induction-type coilguns. The paper starts with a derivation of closed-form formulas which relate the dimensions of the gun to the performance expressed in terms of propulsive and local maximum forces on the projectile, power factor and efficiency of the system, thermal stress of the projectile armature, distributions of the flux density around the launcher, and the system parameters in a multisection coilgun. The paper ends with a numerical example.

1. INTRODUCTION

Various types of electromagnetic coilguns [1-8] have received increased attention recently because they have better characteristics than other electromagnetic launchers. Major advantages of the coilgun include the distribution of mechanical stresses that makes it possible to accelerate heavy projectiles, and the absence of current-carrying contact between barrel and projectile that increases the survivability of the barrel. This paper discusses the design and performance analysis of the induction type coilgun based on a current sheet representation.

The current sheet model replaces the currents in an actual barrel and in a cylindrical tubular projectile (sleeve) with two equivalent current sheets located at their equivalent radii (Fig.1). Since the coils in the barrel of an EM launcher consist either of stranded conductors, or of many series-connected turns, the current distribution may be considered as uniform. The sleeve, on the other hand, is made of a solid conductor and therefore the skin-effect should be considered. However, for the best utilization of sleeve material, the thickness of the sleeve should always be chosen so that the distribution of current is relatively uniform in the radial direction. This implies that the skin-effect in the radial direction of both the barrel coils and the sleeve may be neglected. The actual current distributions in the barrel and in the sleeve can be reduced to cylindrical surface current sheets by letting the thickness of the conductor vanish while letting the current density (A/m^2) go to infinity. With a good approximation, these radii may be taken as the average between the inner and the outer radius of the barrel coils and of the sleeve. In the cylindrical current sheet model shown in Fig. 1, K_b (m/s) and K_s represent the surface current densities in the barrel coils and in the sleeve respectively.

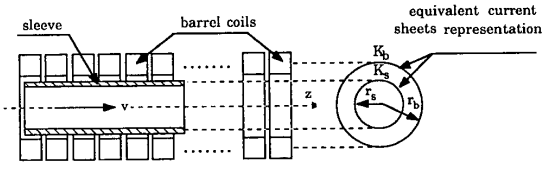

Fig. 1 Transition to current sheet model

The advantage of the current sheet model is that it allows one to obtain simple relations for system analysis and design. The paper starts with a discussion of the current induced in the sleeve; then follows a derivation of expressions for the propulsive force, the power factor of the coilgun, and the distribution of flux density around the coilgun. Multisection system parameters, temperature rise in the sleeve and a numerical example are also discussed in the paper.

2. CURRENT INDUCED IN THE SLEEVE

The excitation current in the barrel may be represented by a surface current density K_b, located at an effective radius r_b and directed azimuthally as shown in Fig. 1. Assuming a traveling-wave form and phasor notation, one can write:

$$\mathbf{K}_b = K_b \cos(\omega t - \beta z)\,\theta_0 = \mathrm{Re}\left\{\underline{K}_b e^{j(\omega t-\beta z)}\right\}\theta_0 \qquad (1)$$

where ω and $\beta=\pi/\tau$ are the radian frequency and wave number of the wave respectively. The complex surface current density $\underline{K}_b$ in Eq. 1 may be selected as the reference phasor, i.e. $\underline{K}_b = K_b(1+j0)$. Neglecting the displacement current and end effects, one can show that the azimuthal component of the magnetic vector potential $\underline{A}^b_\theta$ corresponding to this current density, satisfies the equation

$$\frac{d^2\underline{A}^b_\theta}{dr^2} + \frac{1}{r}\frac{d\underline{A}^b_\theta}{\partial r} - \left(\beta^2+\frac{1}{r^2}\right)\underline{A}^b_\theta = 0 \qquad (2)$$

with boundary conditions

$$\underline{H}_z\left(r_b^+\right) - \underline{H}_z\left(r_b^-\right) = \underline{K}_b$$

$$\underline{B}_r\left(r_b^+\right) = \underline{B}_r\left(r_b^-\right) \qquad (2a)$$

$$\underline{A}(\infty) = 0 \quad \text{and} \quad \underline{A}(0) = \text{finite}$$

where $\mathbf{H}=\mathbf{B}/\mu_0$ and $\mathbf{B}=\nabla\times\mathbf{A}$.

The solution of Eq. (2) is

$$\underline{A}^b_\theta = \begin{cases} \mu_o \underline{K}_b r_b I_1(\beta r_b) K_1(\beta r) & r_b \le r < \infty \\ \mu_o \underline{K}_b r_b K_1(\beta r_b) I_1(\beta r) & 0 \le r \le r_b \end{cases} \qquad (3)$$

where I_1 and K_1 are modified Bessel functions. Similarly, if v denotes the velocity of the sleeve with respect to the barrel, and if one assumes that the surface current density induced in the sleeve $\underline{K}_s$ is located at the effective radius r_s as shown in Fig. 1, one can also obtain the magnetic vector potential $\underline{A}^s_\theta$ due to the induced sleeve current sheet as

$$\underline{A}^s_\theta = \begin{cases} \mu_o \underline{K}_s r_s I_1(\beta r_s) K_1(\beta r) & r_s \le r < \infty \\ \mu_o \underline{K}_s r_s K_1(\beta r_s) I_1(\beta r) & 0 \le r \le r_s \end{cases} \qquad (4)$$

It should be noted that, in the induction-type coilgun, the surface current density induced in the sleeve $\underline{K}_s$ is an unknown variable. It can be determined by considering the field contributions due to both current sheets $\underline{K}_b$ and

0018-9464/91/0100-0579$01.00 © 1991 IEEE

$\underline{K}_s$ at radius r_s, or

$$\underline{K}_s = a_s\gamma_s\left(\underline{E}_\theta^b + \underline{E}_\theta^s + v(\underline{B}_r^b + \underline{B}_r^s)\right) \quad (5)$$

where a_s and γ_s are the sleeve thickness and conductivity respectively; $\underline{E}_\theta^b$ and $\underline{E}_\theta^s$ are the azimuthal components of the electric field intensities at the sleeve boundary ($r=r_s$); $\underline{B}_r^b$ and $\underline{B}_r^s$ are the radial components of the magnetic flux density at the sleeve boundary. Making use of relations $\underline{E}_\theta = -j\omega\underline{A}_\theta$, $\underline{B}_r = j\beta\underline{A}_\theta$, and Eqs. (3) and (4), one can rewrite Eq. (5) as

$$\underline{K}_s = -j\beta a_s\gamma_s v_s\mu_0\left[\underline{K}_b r_b K_1(\beta r_b)I_1(\beta r_s) + \underline{K}_s r_s K_1(\beta r_s)I_1(\beta r_s)\right] \quad (5a)$$

where v_s is the synchronous velocity and $s=(v_s-v)/v_s$ is the slip between the wave velocity v_s and the sleeve velocity v. Solving Eq. (5a) for $\underline{K}_s$, one obtains

$$\underline{K}_s = \frac{-s}{\sqrt{s_c^2+s^2}}\frac{r_b K_1(\beta r_b)}{r_s K_1(\beta r_s)}\underline{K}_b \angle\phi \quad (6)$$

where ϕ is the phase shift between the sleeve current sheet and the barrel current sheet

$$\phi = \tan^{-1}\frac{s_c}{s} \quad (7)$$

and s_c is the critical slip at which the propulsive force reaches its maximum value, as in conventional induction machines

$$s_c = \frac{1}{\mu_o\gamma a_s v_s \beta r_s K_1(\beta r_s)I_1(\beta r_s)} \quad (8)$$

For $\beta r_s >> 1$, the Bessel functions K_1 and I_1 can be approximated by exponential functions [9]. Hence, Eq. (8) can be simplified as

$$s_c = \frac{2}{\mu_o\gamma a_s v_s} \quad (8a)$$

Eq. (8) or (8a) relate the critical slip directly to the sleeve conductivity, and thickness, and to the wave velocity. It is seen from Eq. (7) that the current induced in the sleeve lags the barrel excitation current by an angle varying from 90 to 180 degrees. For small values of s, the amplitude of the sleeve current is approximately proportional to the slip s and for small values of s_c it reaches a maximum value near s=1 i.e. "at standstill". The ratio of the amplitude of the sleeve surface current density K_s to that of the barrel K_b depends on the normalized gap length βg ($=\pi g/\tau$) as shown in Fig. 2. It can be seen that the sleeve current decays almost linearly as βg increases. For a given βg the sleeve current strongly depends on s/s_c.

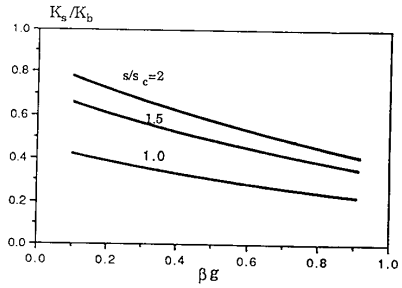

Fig. 2 Current ratio K_s/K_b as a function of the normalized equivalent air-gap $\beta g=\beta(r_b-r_s)$ with s/s_c as parameter. $\beta r_s=1$.

3. PROPULSIVE FORCE ON THE SLEEVE

The propulsive force is given by the product of the current induced in the sleeve $\underline{K}_s$ times the radial component of flux density $\underline{B}_r$. At the sleeve boundary $r=r_s$, $\underline{B}_r$ can be obtained from Eqs. (4), (5) and (6) as

$$\underline{B}_r = j\beta\left(\underline{A}_\theta^b + \underline{A}_\theta^s\right) = \frac{s_c}{\sqrt{s_c^2+s^2}}\mu_o\beta r_b I_1(\beta r_s)K_1(\beta r_b)\,K_b\angle\phi \quad (9)$$

Using Eq. (6) and (9) one can obtain the local force density (N/m^2) acting on the sleeve as a function of time and space.

$$f_z = -K_s(z,t)\,B_r(z,t) = F_{z,m}\{\cos[2(\omega t-\beta z+\phi)]+1\} \quad (10)$$

where the amplitude $F_{z,m}$ is

$$F_{z,m} = \frac{s\,s_c}{s_c^2+s^2}\frac{\mu_o\beta r_b^2 K_1^2(\beta r_b)I_1(\beta r_s)}{2r_s K_1(\beta r_s)}K_b^2 \quad N/m^2 \quad (11)$$

It can be seen from Eq. (10) that the peak of the surface force density is twice that of the time-average force. Also, the propulsive force varies with the slip s. At the critical slip s_c, it reaches a maximum value

$$F_{z,max} = \frac{\mu_0\beta r_b^2 K_1^2(\beta r_b)I_1(\beta r_s)}{4r_s K_1(\beta r_s)}K_b^2 \quad (12)$$

The normalized maximum force density $F_{z,max}/(\mu_0 K_b^2/4)$ is plotted in Figs. 3 and 4. Figure 3 shows its dependence on the normalized sleeve radius βr_s, with the normalized air-gap βg as a parameter, and Fig. 4 shows its dependence on the pole-pitch τ, with r_s as a parameter. It appears that a small g and a large r_s are always preferred in order to get a large propulsive force. However according to Fig. 4, for given g and r_s, there exists a value for the pole-pitch τ that maximizes the propulsive force. For g=1 cm, and r_s varying from 2 cm to 8 cm, the pole pitch should be chosen around 15 cm and not less than 10 cm.

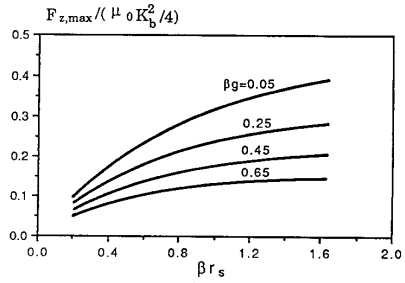

Fig. 3 Dependence of $F_{z,max}/(\frac{1}{4}\mu_0 K_b^2)$ on βr_s with βg as parameter

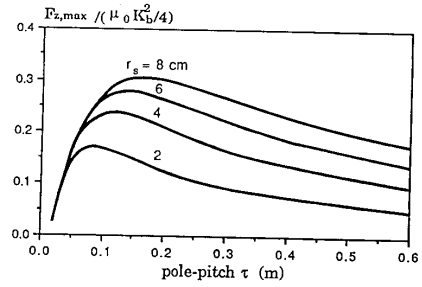

Fig. 4 Dependence of $F_{z,max}/(\frac{1}{4}\mu_0 K_b^2)$ on pole-pitch τ with r_s as parameter (g=1 cm).

4. POWER FACTOR

Generally speaking, the power factor of a coilgun is relatively low because ferromagnetic materials are not used. This means that the stored magnetic energy is much larger than in conventional electrical machines. Limitations and general relations concerning the power factor of air-coil launchers are derived in this section.

The electric field $\underline{E}_\theta$ at the effective radius $r=r_b$ is obtained from Eqs. (3), (4) and (6) as

$$\underline{E}_\theta = v_s \underline{B}_r = j\mu_0 v_s \beta K_1(\beta r_b)\left(\underline{K}_b r_b I_1(\beta r_b) + \underline{K}_s r_s I_1(\beta r_s)\right) \tag{13}$$

$$= \mu_0 v_s \beta r_b K_1(\beta r_b) I_1(\beta r_b) K_b \left[\frac{s\, s_c}{s_c^2+s^2}\Omega + j\left(1 - \frac{s^2}{s_c^2+s^2}\Omega\right)\right]$$

where Ω is

$$\Omega = \frac{I_1(\beta r_s)\, K_1(\beta r_b)}{I_1(\beta r_b)\, K_1(\beta r_s)} \tag{14}$$

Ω may be termed the coupling function of the coilgun since it is a measure of the coupling between the sleeve and the barrel. Ω varies from unity to zero as βg ($=\beta r_b - \beta r_s$) varies from zero to infinity. A normalized air-gap equal to zero ($\Omega = 1$), represents 100% coupling between sleeve and barrel. The variation of Ω as a function of βg and βr_s is shown in Fig. 5. It can be seen from Fig. 5 that Ω decreases sharply as the normalized air-gap βg increases and the normalized radius βr_s decreases. To obtain better coupling between the sleeve and the barrel, one should always choose a small βg, and a large βr_s. For a given pole-pitch τ this means a larger r_s and a smaller g. For large βr_s and βr_b, the coupling function Ω may be simplified by approximating the Bessel functions as exponential functions [9]. Eq. (14) then becomes

$$\Omega = e^{-2\beta g} \tag{14a}$$

From Eq. (13), one can obtain the power factor PF of an induction-type coilgun, i.e. the cosine of the phase shift between $\underline{K}_b$ and $\underline{E}_\theta$

$$PF = \frac{\Omega}{\sqrt{\Omega^2 + \left(\frac{s_c}{s} + \frac{s}{s_c}(1-\Omega)\right)^2}} \tag{15}$$

Figure 6 shows the dependence of power factor on s/s_c with Ω as the parameter. It is seen from Fig. 6 that there exists an optimal value of power factor as s/sc reaches a certain value. Fig. 5 and 6 can be used to determine the relations of the air-gap g, the radius r_s, and the pole pitch τ, or β ($=\pi/\tau$) for a given value of power factor. For instance, if one wishes to obtain a peak power factor of 40%, one can see from Fig. 6 that a Ω of 0.6 is required. But, one can also see from Fig. 5 that in order to obtain an Ω of 0.6, βg must attain the following values: βg=0.05 for βr_s=0.2, βg=0.12 for βr_s=0.5, βg=0.16 for βr_s=0.8, and βg=0.19 for βr_s=1.1.

One can show from Eq. (15) by differentiating with respect to s/s_c that for a given Ω a maximum power factor appears at

$$\frac{s}{s_c} = \frac{1}{\sqrt{1-\Omega}} \tag{16}$$

Substituting Eq. (16) into (15) one obtains the maximum power factor

$$PF = \frac{\Omega}{\sqrt{\Omega^2 + 4(1-\Omega)}} \tag{17}$$

Eq. (17) gives a direct and simple relation between the coupling function and the maximum power factor. From Eqs. (16) and (17) one is able to estimate the power factor and the ratio of s/s_c for a specified value of Ω, or to determine the value of the coupling function Ω for a specified power factor. The ratio of s/s_c is a very important parameter in a multi-section coilgun, a topic which will be discussed in detail later. For larger βr_s and βr_b, one may relate βg directly to the optimal power by using Eqs. (14a) and (17) as

$$\frac{g}{\tau} = \frac{1}{2\pi}\ln\left(\frac{PF+1}{2PF}\right) \tag{18}$$

where $\beta=\pi/\tau$ was used. Eq. (18) can be very useful for estimating the required ratio of the air gap to the pole pitch for a specified power factor. For instance, g/τ should be smaller than 0.0446 (or $\tau/g>22.4$) in order to obtain an optimal power factor larger than 60%.

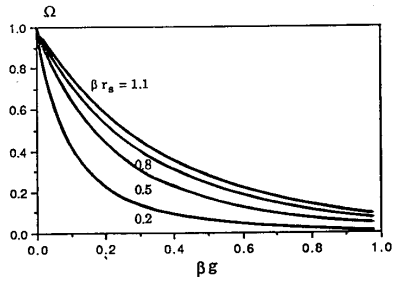

Fig. 5 Coupling function Ω as a function of normalized air gap βg with βr_s as a parameter

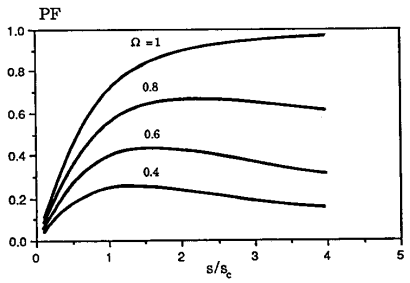

Fig. 6 Dependence of power factor (PF) on s/s_c with Ω as parameter

5. DISTRIBUTION OF THE MAGNETIC FIELD IN THE COILGUN

A coilgun usually operates at a high flux density (above ten Teslas). Since only nonferromagnetic materials are involved in the system, the EM energy is stored everywhere around the launcher. It is very important to find out the distribution of the flux density inside the sleeve, in the air gap, and outside the barrel in order to shield electronic devices near the launcher or in the projectile.

Inside the sleeve, the radial component of the flux density can be directly obtained from Eq. (9) replacing r_s by r. Making using Eq. (3), (4) and (6), one obtains the amplitude of the axial component of the flux density for $r \le r_s$ in term of the radial component

$$B_z(r) = \left(\frac{A_\theta}{r} + \frac{\partial A_\theta}{\partial r}\right) = \frac{I_0(\beta r)}{I_1(\beta r)} B_r(r) \tag{19}$$

The total flux density contributed by both components is then

$$B(r) = \mu_0 K_b \beta r_b K_1(\beta r_b) \frac{s_c}{\left[s^2+s_c^2\right]^{\frac{1}{2}}} \left[I_0(\beta r)+I_1(\beta r)\right]^{\frac{1}{2}} \quad r \le r_s^- \quad (20)$$

Similarly, outside the barrel the amplitude of the flux density can be obtained from Eq. (3), (4), and (6) in terms of the coupling function as

$$B(r) = m_0 \beta r_b I_1(\beta r_b) K_b \left[\frac{s_c^2+s^2(1-W)}{s^2+s_c^2}\right]^{\frac{1}{2}} \left[K_0(\beta r)+K_1(\beta r)\right]^{\frac{1}{2}} \quad r \ge r_b^+ \quad (21)$$

In the air gap ($r_s<r<r_b$)

$$B(r)=\mu_0 K_b \beta r_b K_1(\beta r_b) \times \left\{\frac{\left[s_c^2+s^2(1+\Omega_0)^2\right] I_0^2(\beta r)+\left[s_c^2+s^2(1-\Omega_1)^2\right] I_1^2(\beta r)}{s_c^2+s^2}\right\}^{\frac{1}{2}} \quad (22)$$

where

$$\Omega_0 = \left[1+\frac{I_1(\beta r_s)\, K_0(\beta r)}{K_1(\beta r_s) I_0(\beta r)}\right]^2 \quad \text{and} \quad \Omega_1 = \left[1-\frac{I_1(\beta r_s)\, K_1(\beta r)}{K_1(\beta r_s) I_1(\beta r)}\right]^2$$

It should be noted that the flux density in the air gap is much larger than that inside the sleeve and outside the barrel because its axial component is the sum of contributions from both the sleeve and the barrel current sheets in the air gap. Figure 7 shows the distribution of flux density around the coilgun. As expected, the flux density in the air gap is much higher than that inside the sleeve and outside the barrel. The flux density outside the barrel decays to about 10% of the air gap value after about one barrel diameter. More detailed numerical value will be given in the last section.

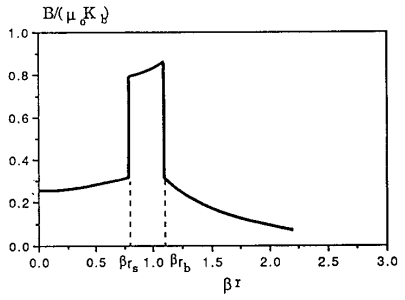

Fig. 7 Normalized flux density vs normalized radius. βr_s=0.8 and βr_b=1.1.

6. MULTISECTION SYSTEM PARAMETERS

To reduce the ohmic loss and, therefore, the temperature rise in the sleeve, it is necessary to operate with a small s. This forces division of the barrel of an induction coilgun into many sections. Every section of the barrel has a different frequency and a different voltage level. To obtain a constant average force on the sleeve in every section of the barrel, it is desirable to have a constant air-gap flux density for every section. This implies that the electric field must be proportional to the frequency. It has been suggested in [10] that for a N_s-section launcher system, one can choose N_s synchronous velocities and N_s-1 exit velocities which minimize the length of the barrel. This involves a set of nonlinear equations with $2N_s$ unknowns the solution of which can be very difficult to obtain if the number of sections is very large. A simplified method that is based on choosing a constant ratio of maximum to minimum force fluctuation for every section is discussed here. The solutions obtained from this simplified method are very close to those obtained from the optimization method.

For the i^{th} section of the barrel, the time-average propulsive force density may be obtained from Eq. (11) and (12) as

$$F_z = \frac{2F_{z,max}}{\frac{s}{s_{c,i}} + \frac{s_{c,i}}{s}} \quad (23)$$

where $s_{c,i}$ is the critical slip in the i^{th} section. Introducing a force fluctuation ratio $\Gamma = F_{z,max}/F_z$ into Eq. (23), one may solve it for s in terms of Γ and $s_{c,i}$ as

$$s_{i-1},\, s_i = s_{c,i}\left(\Gamma \pm \sqrt{\Gamma^2-1}\right) \quad (24)$$

where s_{i-1} is the entrance slip and s_i is the exit slip in the section i. From Eq. (24) one may define an average slip $s_{av,i}$ in the i^{th} section

$$s_{av,i} = \frac{1}{2}(s_{i-1}+s_i) = \Gamma\, s_{c,i} \quad (25)$$

It follows from Eq. (25) that the force fluctuation ratio Γ is the ratio of s/s_c when s represents the average slip. This relation is an important parameter as mentioned in previous sections. The entrance velocity v_{i-1} and the exit velocity v_i corresponding to s_{i-1} and s_i can be obtained from Eq. (24) in terms of the critical slip $s_{c,i}$ and synchronous velocity $v_{s,i}$ in i^{th} section

$$v_{i-1,\,i} = v_{s,i}\left[1 - s_{c,i}\left(\Gamma - \sqrt{\Gamma^2-1}\right)\right] \quad (26)$$

This gives a velocity increment in section i

$$\Delta v_i = v_i - v_{i-1} = 2\, v_{s,i} s_{c,i} \sqrt{\Gamma^2-1} \quad (27)$$

It can be seen from Eq. (27) that for a given Γ, the velocity increment depends only on the dimensions, since, according to Eq. (8), the product $v_{s,i}s_{c,i}$ depends only on the dimensions. It follows that for given dimensions of the gun, a constant Γ leads to a constant velocity increment.

If one assumes an equal velocity increment in every section, the required number of sections N_s of an induction coilgun with breech velocity v_b and muzzle velocity v_m can be obtained from Eq. (27) as

$$N_s = \frac{v_m - v_b}{2 s_c v_s \sqrt{\Gamma^2-1}} \quad (28)$$

One may obtain approximately the length of an induction launcher from a slip-average force. Since the slip s varies with position along the barrel, the propulsive force density varies with the slip s and the position as shown in Eq. (23). One can integrate Eq. (23) from the entrance slip to the exit slip to obtain a slip-average propulsive force

$$F_{av} = \frac{1}{s_{i-1} - s_i} \int_{s_i}^{s_{i-1}} \frac{2F_{z,m}}{\frac{s}{s_c} + \frac{s_c}{s}}\, ds = \frac{F_{zm}}{\sqrt{\Gamma^2-1}} \ln\left(\Gamma + \sqrt{\Gamma^2-1}\right) \quad (29)$$

where Eq. (24) was used. Let ξ denote the mass density of the conducting sleeve, and ν the ratio of the overall mass of the projectile to the mass of the conducting sleeve. Then the increment of kinetic energy (per unit volume)

from the breech velocity v_b to the muzzle velocity v_m equals the work done by the electromagnetic force, or approximately equals the product of the force per unit volume F_{av}/a_s and the total barrel length l. This allows one to determine the length of the barrel of an induction-type launcher as

$$l = \frac{1}{2}\nu\xi\,(v_m^2 - v_b^2)\frac{a_s}{F_{av}} \tag{30}$$

After finding the length of barrel from Eq. (30) one can determine the length of each section. This is proportional to the increment of the kinetic energy within the section if one chooses an equal velocity increment Δv in every section. The length of the i^{th} section, l_i, is

$$l_i = \frac{v_i^2 - v_{i-1}^2}{v_m^2 - v_b^2}\,l = \frac{\Delta v^2}{v_m^2 - v_b^2}\,(2i-1)\,l \tag{31}$$

From Eq. (31), it is seen that the length of the first few sections may be too short since the minimum length of the section must be at least two pole pitches 2τ. One solution is to merge the first several sections into one section. This may require the frequency of the source to be increased stepwise in this section. The minimum number of sections needed to be merged is determined from Eq. (31) by letting $l_i = 2\tau$, solving for $i = N_m$ and taking the nearest integer or

$$N_m = \frac{\tau}{l}\frac{v_m^2 - v_b^2}{\Delta v^2} + \frac{1}{2} \tag{32}$$

7. TEMPERATURE RISE IN THE CONDUCTING SLEEVE

In a multisection induction coilgun, the temperature in the sleeve is the sum of contributions from all sections of the barrel. In the i^{th} section the energy dissipated per unit volume of the conducting sleeve $W_{cu,i}$ can be expressed in terms of average slip $s_{av,i}$ and the kinetic energy W_{kin} gained in that section

$$W_{diss} = \frac{s_{av,i}}{(1 - s_{av,i})}W_{kin} = \frac{s_{av,i}}{(1 - s_{av,i})}\frac{1}{2}\nu\xi(v_i^2 - v_{i-1}^2) \tag{33}$$

On other hand, this amount of energy also equals the product of the specific heat c (J/m^3K) and the temperature rise θ_i, from which one can obtain the temperature rise in the i^{th} section as

$$\theta_i = \frac{\nu\xi(v_i^2 - v_{i-1}^2)s_{av,i}}{2c\,(1 - s_{av,i})} \tag{34}$$

Making use of Eq. (25), (27) and the relation $(v_{i-1}+v_i)/2 = (1-s_{av,i})v_{s,i}$ one can rewrite Eq. (34) as

$$\theta_i = \frac{\nu\xi s_{c,i}v_{s,i}\Gamma}{c}\Delta v_i \tag{34a}$$

If we assume a constant velocity increment for every section, so that the temperature rise in every section is same, the cumulative temperature rise in the sleeve when passing through the barrel can be found as

$$\theta = N_s\theta_i = \frac{\nu\xi s_c v_s}{c}\Gamma(v_m - v_b) \tag{35}$$

Substituting Eq. (35) into Eq. (28), one can relate the required number of sections to the temperature rise in the sleeve as

$$N_s = \frac{\nu\xi}{2c\theta}\frac{\Gamma}{\sqrt{\Gamma^2 - 1}}(v_m - v_b)^2 \tag{36}$$

8. NUMERICAL EXAMPLES

To demonstrate the analysis approach developed in this paper for the induction coilgun, a numerical example is given in this section. Assume that the set of specifications for an induction coilgun is:

Initial velocity	v_b	0
Muzzle velocity	v_m	5 km/s
Projectile weight	W_p	0.5 kg
Sleeve material		aluminum

The properties of the aluminum sleeve are:

Mass density	ξ	2700 kg/m^3
Specific heat	c	2.56×10^6 $JK^{-1}m^{-3}$
Temperature rise	θ_m	400° K
Yield stress	σ_m	6.9×10^7 Pa
conductivity	γ	1.63×10^7 S/m

Since the sleeve is not uniformly heated along its length [4], an average temperature rise of 400°K, about half of that required to reach the melting-point of the material, was chosen as the value for the maximum allowable temperature rise.

Starting from Eq. (35) one may choose $\nu=1.3$ and $\Gamma=2$, and obtain

$$s_c v_s = \frac{c\theta}{\nu\xi v_m\Gamma} = 28.9 \text{ m/s}$$

From Eq. (8a) or (8) one obtains the thickness of the sleeve as

$$a_s = \frac{2}{\mu_0\gamma s_c v_s} = 4.4 \text{ mm}$$

If one chooses $\tau=10$ cm and sleeve length $l_s = 2\tau$, the average sleeve radius r_s can be determined

$$r_s = \frac{W_p}{2\pi a_s l_s \xi\nu} = 2.6 \text{ cm}$$

The required number of barrel sections, $N_s=50$, is obtained from Eq. (28). The total length of the barrel is determined from Eq. (30). By choosing an average propulsive force density $F_{av}=10^7$ N/m^2 one gets $l=19.3$ m. One can obtain the length of each section from Eq. (31). The number of sections required to be merged is given by Eq. (32), $N_m=13$. This shows that the actual number of sections the system involves is about $N_s-N_m=37$ sections.

From Eq. (29) one can obtain the maximum induction surface force density $F_{z,max}=1.32\times10^7$ N/m^2 where the equivalent air-gap g=8 mm was used. The required barrel current sheet is obtained from Eq. (12) $K_b=1.4\times10^7$ A/m, or 0.99×10^7 A/m in rms value. The induced sleeve current sheet is given by Eq. (6) $K_s=0.752\,K_b$ with a phase delay of 153.4 degrees.

The value of the coupling function $\Omega = 0.464$ is determined from Eq. (14) or (14a), and the power factor of the gun PF= 28.3% from Eq. (15). It is noted that the power factor may be increased by choosing a larger pole pitch and barrel radius as shown in Eqs. (14) and (15).

Flux density was obtained from Eqs. (20), (21) and (22): B=15 T in the air gap; B=4.9 T in the center of the sleeve; and B < 1 T outside the barrel beyond one barrel radius.

The electric field intensity in the barrel coils is given by Eq. (13). Using the dimensions and specifications in this example, one obtains an electric field in the last section

$$E_\theta = v_s B_r = 0.231\mu_0 K_b v_s = 21 \text{ kV/m}$$

where $v_s=5100$ m/s was used. This gives a voltage per turn in rms value

$$V/N=21(2\pi r_b)/\sqrt{2} = 2428\ V$$

If we choose 3.5 cm for the coil width, we obtain the rms ampere-turns for the barrel coils as

$$NI=0.035K_b=346.5\ kA\ turns.$$

9. CONCLUDING REMARKS

This paper is based on the assumption that a quasi-steady state prevails during the operation of the coilgun, i.e. that the mechanical time constants are much larger than the electrical ones. In this regime the paper provides guidelines for the design of coilguns, and its closed form formulas are advantageous in the optimization procedures.

With high accelerations, and with energization by means of capacitors banks, electrical transients cannot be neglected. An approach based on computer simulation of these transients is presented in a companion paper [11].

ACKNOWLEDGMENT

This work was sponsored by SDIO/IST and managed by USASDC, contract No. DASG60-88-C-0047.

REFERENCES

1. T. J. Burgess, E. C. Cnare, W. L. Oberkampf, S. G. Beard and M. Cowan, "The Electromagnetic Theta Gun and Tubular Projectiles", IEEE Transactions on Magnetics, Vol. MAG-18, No. 1, Jan. 1982 pp. 46-59.
2. P. Mongeau and F. Williams, "Arc-Commutated Launcher," IEEE Transactions on Magnetics, Vol. MAG-18, No. 1, Jan. 1982, pp. 42-45.
3. M. D. Driga, W. F. Weldon, and H. H. Woodson, "Electromagnetic Induction Launchers," IEEE Transactions on Magnetics, Vol. MAG-22, No. 6, Nov. 1986 pp. 1453-1458.
4. J. L. He, E. Levi, Z. Zabar and L. Birenbaum, "Concerning the Design of Capacitively-Driven Induction Coil-Guns," IEEE Transactions on Plasma Science, June 1989, Vol. 17, No. 3, pp. 429-438.
5. M. Cowan, E. C. Cnare, B. W. Duggin, R. J. Kaye and T. J. Tucker, "The Reconnection Gun," IEEE Transactions on Magnetics, Vol. MAG-22, No. 6, Nov. 1986, pp. 1429-1434.
6. D. G. Elliott, "Traveling-Wave Induction Launchers", IEEE Transaction on Magnetics, Vol. 25, No. 1, Jan. 1989, pp. 159-163.
7. P. Mongeau, "Inductively Commutated Coilguns", 5th Symposium on Electromagnetic Launcher Technology, Sendestin, Florida, April 2-5, 1990.
8. D. G. Elliott, "Study of Advanced Electromagnetic Launchers," Progress Report No. 5, JPL D-5413, Jet Propulsion Laboratory, Pasadeno, CA.
9. J. Spanier and K. B. Oldham, "An Atlas of Functions," Hemisphere Publishing Corporation, 1987.
10. T. Onuki, E. R. Laithwaite, "Optimised Design of Linear-Induction-Motor Accelerator," IEE Proceedings, Vol. 118, No. 2, Feb. 1971, pp. 349-355.
11. J. L. He, Z. Zabar, E. Levi and L. Birenbaum, "Transient Performance of Linear Induction Launchers Fed by Generators and by Capacitor Banks," 5th Symposium on Electromagnetic Launcher Technology, Sandestin, Florida, April 2-5, 1990.